Fragment-derived inhibitors of human *N*-myristoyltransferase block capsid assembly and replication of the common cold virus

Authors

Aurélie Mousnier[1,2,†], Andrew S. Bell[3,†], Dawid P. Swieboda[1], Julia Morales-Sanfrutos[3], Inmaculada Pérez-Dorado[3,4], James A. Brannigan[5], Joseph Newman[6], Markus Ritzefeld[3], Jennie A. Hutton[3], Anabel Guedán[1], Amin A. Asfor[6], Sean W. Robinson[7], Iva Hopkins-Navratilova[7,8], Anthony J. Wilkinson[5], Sebastian L. Johnston[1], Robin J. Leatherbarrow[3,‡], Tobias J. Tuthill[6], Roberto Solari[1]*, Edward W. Tate[3]*

Affiliations

1. National Heart & Lung Institute, St Mary's Campus, Praed Street, London W2 1NY, UK
2. Centre for Experimental Medicine, Queen's University Belfast, 97 Lisburn Road, Belfast BT9 7BL, UK
3. Department of Chemistry, Imperial College London, London SW7 2AZ, UK
4. Department of Life Sciences, Imperial College London, Exhibition Road, London SW7 2AZ, UK
5. Structural Biology Laboratory, Department of Chemistry, University of York, York YO10 5DD, UK
6. The Pirbright Institute, Ash Road, Pirbright, Woking, GU24 0NF, UK
7. Kinetic Discovery Limited, 14 City Quay, Dundee, DD1 3JA, UK
8. School of Life Sciences, University of Dundee, Dow Street, Dundee, DD1 5EH, UK

†: A.M. and A.S.B. contributed equally to the work described here.

‡: Current address: Liverpool John Moores University, Egerton Court, 2 Rodney Street, Liverpool, L1 2UA, UK

Abstract

Rhinoviruses are the pathogens most often responsible for the common cold, and are a frequent cause of exacerbations in asthma, chronic obstructive pulmonary disease and cystic fibrosis. Here we report discovery of IMP-1088, a picomolar dual inhibitor of the human *N*-myristoyltransferases NMT1 and NMT2, and use it to demonstrate that pharmacological inhibition of host cell *N*-myristoylation rapidly and completely prevents rhinoviral replication without inducing cytotoxicity. Identification of cooperative binding between weak-binding fragments led to rapid inhibitor optimization through fragment reconstruction, structure-guided fragment linking, and conformational control over linker geometry. We show that inhibition of co-translational myristoylation of a specific virus-encoded protein (VP0) by IMP-1088 potently blocks a key step in viral capsid assembly, delivering low nanomolar antiviral activity against multiple rhinovirus strains, poliovirus and foot-and-mouth disease virus, and protection of cells against virus-induced killing, highlighting the potential of host myristoylation as a drug target in picornaviral infections.

Main Text

Rhinovirus (RV) is the pathogen most often responsible for the common cold, and is the most frequent cause of exacerbation and morbidity in important respiratory diseases including asthma, chronic obstructive pulmonary disease (COPD)[1], and cystic fibrosis[2,3]. It is a member of the *Picornaviridae* family that includes other important human and animal pathogens such as poliovirus (PV), foot-and-mouth disease virus (FMDV), coxsackievirus, hepatitis A virus and enterovirus 71 (EV-A71). Despite the importance of RV as a pathogen in respiratory diseases, a specific treatment is lacking. On the one hand, massive RV serotypic diversity (over 100 serotypes are known) precludes generation of broad-spectrum vaccines, whilst rapid

emergence of resistance has been observed for previous inhibitors targeting the virus itself, thanks to its rapid replication and high mutation rate[4].

The RNA genome of RV is translated by host ribosomes into a single polyprotein (Fig. 1a) that is processed by viral proteases to form the capsid precursor protein, and a number of non-structural proteins required for completion of the viral life cycle[5]. The capsid precursor is further processed into three capsid proteins VP0, VP3 and VP1 (Fig. 1b), triggering a cascade of protein self-assembly which ultimately leads to formation of infectious virions. This cascade starts with formation of a VP0/VP1/VP3 complex termed a protomer; five protomers assemble into pentamers, and twelve pentamers and the viral RNA genome then assemble to form an icosahedral virion[6]. The final maturation step involves cleavage of VP0 into VP4 and VP2, in the intact viral capsid.

VP0 is encoded at the N-terminus of the viral polyprotein (Fig. 1a), and in many picornaviruses is *N*-myristoylated by host cell *N*-myristoyltransferase (NMT). NMT undertakes transfer of myristate from myristoyl coenzyme A (Myr-CoA) to the N-terminus of a range of proteins during protein translation (i.e. co-translationally), and is widely conserved across all eukaryotic species[7], with higher organisms such as humans expressing two NMT proteins (NMT1 and NMT2) in most tissues. Mutagenesis studies in poliovirus suggest that VP0 *N*-myristoylation plays a role in capsid assembly and infectivity[8-11], and host NMT may therefore be an attractive antiviral drug target that is minimally susceptible to both serotypic variation and the propensity of the virus to mutate, since host NMT is an invariant factor in viral replication.

Here we report the development of a novel class of dual human NMT1/2 inhibitors through a fragment reconstruction and linking approach which delivers a 100,000-

fold improvement in potency, and the first picomolar inhibitors of the human enzymes. We use these compounds to demonstrate that pharmacological inhibition of VP0 myristoylation by NMT in the host cell results in a specific failure to assemble virions, leading to complete suppression of RV replication and infectivity, and confirm the essentiality of VP0 myristoylation for RV viability through mutagenesis. We show that this mode of action is widely efficacious across multiple RV strains, in primary tissue models, against poliovirus and FMDV, and prevents virus-induced cytotoxicity in host cells, indicating the potential of the human NMTs as broad spectrum antipicornaviral drug targets.

Results

A fragment reconstruction and merging approach leads to a picomolar human NMT inhibitor

NMT inhibitors to date, including those reported by our labs, have been developed primarily against NMT in protozoan parasites or fungi[12], and compounds in these inhibitor series only modestly reduce protein *N*-myristoylation in human cells[13]. We reasoned that a new series optimized specifically against the human NMTs could deliver greatly improved cellular activity, and a tool with which to explore the anti-rhinoviral potential of NMT inhibition. During exploration of hits from a high-throughput screen against NMT from the human malaria parasite *Plasmodium falciparum*[14], we identified a novel fragment-like compound IMP-72 (Fig. 2a) with weak but measurable activity against human NMT1 (HsNMT1, IC_{50} 20 μM). The binding mode of this fragment was initially determined in NMT from malaria parasite *Plasmodium vivax* (PvNMT) in the presence of a non-hydrolysable myristoyl CoA analogue (NHM)[15] (Fig. 2b; see Supplementary Fig. 1 for ligand electron density maps). IMP-72 was found to interact through its dimethylamine with the C-terminal

carboxylate of the enzyme, a residue essential for catalytic activity. However, IMP-72 also makes a novel interaction through the phenyl ring to displace a tyrosine residue in the active site (Y211 in PvNMT); since this residue is conserved in human NMT (Y296 in HsNMT1), we considered IMP-72 a promising starting point for development of an inhibitor of the human enzymes.

We noted that IMP-72 binds in a region complementary to a quinoline inhibitor previously reported by our labs (MRT00057965, Supplementary Fig. 1)[16] and exploits distinct interactions, suggesting an opportunity for rapid optimization through fragment merging. However, on examination of the overlaid binding modes it was evident that the two fragments would clash unfavorably in the active site of the enzyme (Supplementary Fig. 1). We therefore reconstructed MRT00057965 as a simplified quinoline fragment (IMP-358) which we hypothesized would recapitulate the key interaction of MRT00057965 with a conserved serine (S319 in PvNMT, S405 in HsNMT1) at the base of the pocket, without clashing with IMP-72. At a concentration of 100 μM this weakly-binding fragment showed only 17% inhibition of HsNMT1. However, in the presence of 100 μM IMP-358 the potency of IMP-72 was increased >25-fold for PvNMT (to <5 nM) and 300-fold for HsNMT1 (to 65 nM), suggesting a remarkable synergism between these distinct binding modes. The potential for cooperative binding was supported by a quaternary X-ray structure of PvNMT in complex with IMP-72, IMP-358 and NHM, in which the fragments adopt complementary binding sites (Fig. 2c and 2d). Taken together, these data suggest that binding of IMP-72 presents an optimal cavity for binding of IMP-358, delivering synergistic inhibition ideal for fragment linking.

We next sought to replace the quinoline with a more ligand efficient motif to improve both solubility and potency, whilst developing a strategy to link the fragments through

the phenyl ring of IMP-72. An ether linker combined with a trimethylpyrazole resulted in a synthetically tractable route to IMP-917, a dual HsNMT1/2 inhibitor with >1000-fold improved potency over IMP-72 (Fig. 2a). Parallel optimization of the IMP-72 indazole core by *N*-methylation improved chemical stability by reducing the potential for elimination of dimethylamine, whilst also delivering a modest improvement in potency (IMP-994, Fig. 2a). Inspection of the binding mode of IMP-917 in human NMT1 with the co-substrate Myr-CoA (Fig. 2e) revealed that the first two atoms of the ether linker lie in the plane of the phenyl ring; this conformation has previously been proposed to be inherent to this motif[17], and exerts a suboptimal interaction with HsNMT1. Moving the fluorine substituent on the phenyl ring to flank the linker yielded IMP-1031 (Fig. 3a), a single digit nM IC_{50} dual human NMT1/2 inhibitor; crystallography confirmed that the linker is forced into an out-of-plane conformation, optimizing the interaction with S405 (Supplementary Fig. 1). Finally, reintroduction of the fluorine substituent present in the original IMP-72 core resulted in IMP-1088, a sub-nanomolar IC_{50} inhibitor of human *N*-myristoyl transferases HsNMT1 and HsNMT2 (Fig. 3b). A high resolution (1.88 Å) X-ray structure with HsNMT1 and the cofactor myristoyl-CoA (Fig. 3b) shows that IMP-1088 forms an extensive network of interactions in the protein substrate pocket, supporting its unprecedented potency. Indeed, IMP-1088 is sufficiently potent to be beyond the sensitivity of enzyme inhibition assays, suggesting tight binding in the picomolar range[18]. The difluorophenyl indazole linker takes a unique trajectory through the enzyme active site, displacing the Y296 side chain; in this more exposed conformation the tyrosine ring stacks over the inhibitor, resulting in a deeply buried ligand binding mode. Furthermore, the ether linker is twisted out of plane as designed, enabling the pyrazole ring to form a strong hydrogen bond with S405, and inducing an alternative

conformation for H298 by comparison with IMP-917 (Supplementary Fig. 1), as well as stacking and hydrophobic interactions with the side chains of V181, F188, F190, and F311. The interactions of IMP-917 and IMP-1088 with HsNMT1 were further compared by surface plasmon resonance (SPR) to determine the correlation of binding affinity with enzyme inhibition (Supplementary Fig. 2). The measured equilibrium dissociation constants (K_D) of 46 nM for IMP-917 and <210 pM for IMP-1088 were in line with their respective HsNMT1 IC_{50} values, with the latter based on an upper limit for the dissociation rate constant (k_d) due to the extremely slow off-rate of IMP-1088.

Human NMT inhibitors inhibit rhinovirus capsid myristoylation in cells

With an exceptionally potent inhibitor in hand we next explored the impact of IMP-1088 on RV capsid myristoylation in cells, using a chemical proteomic approach which takes advantage of alkyne-tagged myristate analogue, YnMyr (Supplementary Fig. 3)[13,19]. Metabolic labeling with YnMyr over a single-cycle 6-hour synchronous infection with human rhinovirus strain RV-A16 in HeLa cells (multiplicity of infection (MOI) of 20) was followed by copper catalyzed azide-alkyne cycloaddition (CuAAC) of protein lysate to AzTB, an azide capture reagent bearing a TAMRA fluorophore and biotin dual label (Supplementary Fig. 3)[19]. Subsequent SDS-PAGE and in-gel fluorescence analysis revealed a new fluorescent band at the expected molecular weight of VP0 (approximately 37 kDa), superimposed on a band pattern characteristic of NMT-dependent labeling of *N*-myristoylation in HeLa cells (Fig. 3c)[13,20], suggesting that VP0 is myristoylated at 6 hours post-infection. Global identification of proteins for which myristoylation is selectively inhibited by IMP-1088 was performed by quantitative chemical proteomic comparison of YnMyr-tagged proteins in HeLa cells infected with RV, and treated with 50 nM IMP-1088 versus

vehicle (DMSO) treated controls. Proteins were subjected to ligation to AzRB, an azide capture reagent bearing a trypsin-cleavable linker and biotin dual label (Supplementary Fig. 3)[13,21], followed by affinity enrichment on NeutrAvidin beads, on-bead digestion with trypsin, nanoLC-MS/MS analysis of tryptic peptides, and data processing by label-free protein quantification (LFQ) in MaxQuant[22,23]. LFQ intensities across replicates were highly reproducible (R^2 = 0.96-0.98, n = 3), and permutation-based false discovery rate (FDR) two sample *t*-tests were used to compare inhibitor-treated samples with controls. Multiple *N*-myristoylated proteins were identified in enriched samples, including the RV polyprotein which was significantly less enriched in the presence of IMP-1088 (Fig. 3d). Global proteome analysis in the same samples showed no significant changes in protein abundances across the whole proteome in the presence of IMP-1088, consistent with NMT inhibitor-dependent reduction in enrichment (Supplementary Fig. 4). Inhibition of capsid myristoylation was further validated by Western blot with an antibody recognizing rhinovirus VP0 and VP2 (Fig. 3e), whereby the amount of tagged protein pulled down was dose-dependently reduced by IMP-1088 while the total abundance of protein was unaltered. The majority of viral capsid peptides identified in the pull-down mapped to the VP0 domain of the polyprotein, and the N-terminal YnMyr-tagged peptide was readily identified by MS/MS (Supplementary Figs. 5 and 6). These data provide the first direct proteomic evidence for RV capsid myristoylation in human cells and demonstrate that this lipid modification is susceptible to inhibition by a potent NMT inhibitor.

NMT inhibition blocks production of infectious picornaviruses and protects cells from virus-induced cytotoxicity

We next evaluated the ability of NMT inhibitors to rescue host cells from the cytopathic effect (CPE) caused by rhinovirus replication. HeLa cells were infected with RV-A16 at low MOI (0.5) for 2 days, allowing several rounds of virus replication in the presence of NMT inhibitor (or DMSO vehicle control), whereupon cell viability was measured to quantify virus-induced CPE. We compared IMP-1088 with the less potent analogue IMP-1031 and found that both compounds prevented virus-induced CPE in a dose-dependent manner (Fig. 4a), with IC_{50} values of 17 nM for IMP-1088 (95% confidence interval (CI): 6.3-46 nM) and 64 nM for IMP-1031 (95% CI: 37-114 nM), in line with their relative potencies against recombinant HsNMT. In contrast, IMP-994 had no effect on CPE, as expected for a weak (9 µM HsNMT1 IC_{50}) inhibitor (Supplementary Fig. 7). The absence of target engagement for this inactive control molecule in HeLa cells was further confirmed by YnMyr tagging experiments across a wide range of concentrations, in comparison to target engagement observed for IMP-1088 at low-nM concentration (Supplementary Fig. 7). Notably, none of these compounds had any effect on cell viability measured in parallel in uninfected cells, under the same conditions (Fig. 4b and Supplementary Fig. 7). This observation is in line with previous studies showing that low cytotoxicity during acute NMT inhibition reflects the relatively slow turnover of human NMT substrates[13,20], providing a substantial window between antiviral efficacy and host cell toxicity. The very slow off-rate of IMP-1088 may result in extended NMT inhibition in cells, with a potential risk of long-term cytotoxicity; however, this would be counteracted by recovery from inhibition through NMT re-synthesis. To test recovery from NMT inhibition, we treated HeLa cells with IMP-1088 for 24 h, followed

by wash-out of compound and measurement of in-cell NMT activity (with YnMyr) and cell viability 24 h later (Supplementary Fig. 8). NMT activity fully recovered by 24 h, and no cytotoxicity was detected at any time point, confirming the capacity of cells to recover from transient NMT inhibition.

The effect of the more potent inhibitor (IMP-1088) was confirmed in a complementary assay measuring the titer of infectious virus produced in a single-cycle of infection (Fig. 4c); complete suppression of new infectious virus was observed at 125 nM IMP-1088, with a similar IC_{50} to the multicycle replication assay (5.8 nM; 95% CI: 1.6-15 nM). The antiviral potency of IMP-1088 against RV-A16 was maintained against a range of different RV serotypes (Fig. 4d), and against the picornaviruses poliovirus and FMDV (Supplementary Fig. 9), consistent with inhibition of conserved and essential modification of VP0 by host NMT. Furthermore, IMP-1088 blocked production of infectious virus in primary human bronchial epithelial cells (hBEC), a model more representative of human infection (Fig. 4e), and this inhibition was fully maintained during co-administration of the glucocorticoid receptor agonist fluticasone propionate, a standard inhaled corticosteroid for patients with COPD and asthma (Supplementary Fig. 10)[24]. Remarkably, IMP-1088 significantly inhibited production of infectious virus even when added up to 3 hours post-infection, suggesting efficacy can be maintained even in the face of an active infection (Fig. 4f).

In addition to demonstrating the impact of NMT inhibition on infectious virus production, these data strongly indicate that VP0 myristoylation is essential for production of infectious RV virus, as previously observed for poliovirus[8]. We generated a RV construct allowing the expression of the RV polyprotein with a Glycine at position 2 mutated to an Alanine (G2A) at the N-terminus to block VP0 *N*-

myristoylation. As expected, this mutation prevented recovery of viable virus (Supplementary Fig. 11), consistent with the hypothesis that VP0 myristoylation is required for formation of infectious virus particles.

NMT inhibition prevents assembly of intact virions

We next sought to determine the mechanism of antiviral activity. Interestingly, even though no new infectious virions are produced under NMT inhibition (Fig. 5a), IMP-1088 blocked neither production of viral RNA (Fig. 5b), nor translation of rhinovirus polyprotein (Fig. 5c and d), an outcome which was conserved in primary hBECs (Supplementary Fig. 12). These data suggest that the key step mediating NMT inhibitor efficacy lies between protein translation and production of infectious virions. Since processing of viral polyprotein appeared to be unaffected (Fig. 5c), we investigated the effect of IMP-1088 on virus assembly itself by fractionating cell lysates from infected cells on a sucrose density gradient to separate viral assembly intermediates, and analyzing fractions by Western blotting with an anti-rhinovirus capsid antibody. In DMSO-treated controls capsid proteins were detected in intact virion and empty capsid fractions; the latter represent capsids which have formed without packaging the RNA genome, and are commonly observed in cells containing rapidly replicating virus. However, in IMP-1088 treated cell lysates, capsid proteins were detected predominantly in unassembled monomer/pentamer fractions (Figs. 5e and 5f), whilst assembled virions were essentially undetectable, indicating that IMP-1088 blocks virus assembly. Western blot analysis of cell lysates from infected cells revealed a marked decrease in the amount of VP2 protein detected under NMT inhibition, while the total amount of other capsid proteins remained similar (Supplementary Fig. 13). Since the maturation cleavage of VP0 to generate VP4 and

VP2 only occurs in fully assembled particles[25], the absence of VP2 further supports the conclusion that NMT inhibition blocks the assembly of infectious virus.

Discussion

The results described here establish a new series of human NMT inhibitors, discovered through an unusual fragment reconstruction approach starting from two very weak HsNMT inhibitors identified in high-throughput screens against heterologous parasite targets. By leveraging crystallographic binding modes determined in the parasite NMTs we constructed fragment-like compounds with remarkable cooperative inhibitory effects, and complementary binding modes as revealed in the structure of a quaternary complex of both fragments with HsNMT1 and a co-substrate analogue. The perfectly poised binding modes of these fragments enabled rapid fragment linking optimization guided by crystallography at each step, firstly by improving a key H-bond acceptor, and subsequently controlling linker conformation to deliver IMP-1088, an exceptionally potent HsNMT1/2 dual inhibitor. Although the enzyme inhibitory potency of IMP-1088 lies beyond the effective range of an enzyme activity assay, subsequent antiviral studies in cells and SPR studies together suggest an IC_{50} of approximately 200 pM for IMP-1088 against HsNMT1/2. We anticipate that IMP-1088 will be an excellent probe to enable future studies of the role of NMT and *N*-myristoylation in human cell and disease biology, as exemplified by the work reported here on picornaviral replication.

Multiple lines of evidence support the hypothesis that IMP-1088 effectively and potently inhibits production of infectious rhinovirus virions by blocking rhinovirus VP0 *N*-myristoylation. Using a powerful chemical tagging approach in cells infected with RV, we demonstrate a specific impact of IMP-1088 on *de novo N*-myristoylation of

NMT substrate proteins with no impact on protein synthesis, confirming selective target engagement by IMP-1088. This chemical proteomic analysis also provides the first direct evidence for *N*-myristoylation of RV VP0, confirming it as a substrate of host NMT. We used IMP-1088 as a chemical probe to demonstrate the critical role of VP0 myristoylation in virion assembly, particularly in the transition to intact capsids, suggesting that the myristate group is important for aggregation of protomers and pentamers. This hypothesis is in line with genetic studies in poliovirus[8-11], and is fully consistent with the results reported here on an RV VP0 mutant, further supporting the selectivity of IMP-1088 and providing the first unambiguous pharmacological evidence for NMT as a highly effective antipicornaviral target.

In keeping with its specific mode of action, NMT inhibition has no impact on viral RNA replication or polyprotein synthesis, nor does it impact host cell viability over the course of infection. Indeed, thanks to its potent antiviral activity, IMP-1088 is highly effective in *protecting* host cells from the cytotoxic effects of viral infection. Previous studies of the role of NMT in cancer cell lines[13,20] support the hypothesis that the large efficacy window between host and virus is a result of substantial differences in the rate of protein turnover. At the point of inhibitor treatment, pre-existing *N*-myristoylated host proteins must be degraded before an impact on the cell is observed, a process which takes several days[20] compared to a matter of hours for cytotoxicity driven by RV replication. Furthermore, we have shown that NMT activity recovers rapidly following inhibitor wash-out, with no long-term effects on cell viability. Together these data suggest that a substantial therapeutic window might exist for a drug targeting NMT in picornaviral infections, provided dosing is undertaken near the start of infection and does not extend beyond the few hours required to suppress replication. In the case of asthma, cystic fibrosis or COPD, we

suggest that this window might be expanded by inhaled delivery of an NMT inhibitor directly to the site of respiratory infection, and by tuning pharmacokinetics to limit systemic stability and thus prevent distribution of active inhibitor beyond the lung. Clearly, extensive toxicological studies will be required in future to determine whether the benefits of efficacy and novel mode of action outweigh the potential risks of targeting the host lipidation machinery. Intervention in RV infection would also need to be coupled to diagnosis in the earliest hours post-infection, methods for which are currently lacking in the clinic. The observation that many picornaviruses have evolved to depend on host myristoylation suggests that this mode of action might circumvent the development of resistance to a drug targeting NMT, since viral mutations would not influence inhibitor potency against a host enzyme. Interestingly, the concept of targeting a core host lipidation process to block viral replication was recently validated in the clinic in a phase 2A trial of an inhibitor of host prenylation of Hepatitis D virus[26].

Our data show that pharmacological NMT inhibition effects complete inhibition of RV replication in both multi-cycle and single-cycle infection assays, across a number of RV serotypes, in HeLa cells and in primary cells, in the presence of a standard of care corticosteroid for asthma and COPD, and in poliovirus and FMDV infections. RV is the most common respiratory virus associated with pulmonary exacerbations and morbidity in asthma and COPD, and in cystic fibrosis, where patients have a high virus burden in the lungs which is associated with a worsening of their condition. The data presented here suggest that human NMT merits further investigation as a drug target in myristoylation-dependent picornavirus infections, with potential applications in the treatment of RV-induced exacerbations of asthma, COPD, cystic fibrosis, and other picornaviral diseases.

Methods

Details for the synthesis and characterization of all compounds, crystallography, biochemistry, cell biology and virology, protein labeling and proteomics are provided in Supplementary Information.

Data Availability Statement

All relevant data are available from the authors, and 3D structure coordinates and proteomics datasets have been deposited to public repositories, as detailed below.

Accession codes

Primary accessions (Protein Data Bank): 5MU6 (Hs:MYA:IMP-1088); 5O48 (Pv:NHM:IMP-72); 5O4V (Pv:NHM:IMP-72+IMP-358); 5O6H (Hs:MYA:IMP-917); and 5O6J (Hs:MYA:IMP-1031).

The mass spectrometry proteomics data have been deposited to the ProteomeXchange Consortium (http://proteomecentral.proteomexchange.org) via the PRIDE partner repository[27] with the dataset identifier PXD005798.

References

1. Ritchie, A.I. *et al.* Pathogenesis of Viral Infection in Exacerbations of Airway Disease. *Ann Am Thorac Soc* **12 Suppl 2**, S115-132 (2015).
2. Kieninger, E. *et al.* High rhinovirus burden in lower airways of children with cystic fibrosis. *Chest* **143**, 782-790 (2013).
3. Flight, W.G. *et al.* Incidence and clinical impact of respiratory viruses in adults with cystic fibrosis. *Thorax* **69**, 247-253 (2014).
4. Thibaut, H.J., De Palma, A.M. & Neyts, J. Combating enterovirus replication: state-of-the-art on antiviral research. *Biochem Pharmacol* **83**, 185-192 (2012).
5. Jiang, P., Liu, Y., Ma, H.C., Paul, A.V. & Wimmer, E. Picornavirus morphogenesis. *Microbiol Mol Biol Rev* **78**, 418-437 (2014).
6. Liu, Y. *et al.* Atomic structure of a rhinovirus C, a virus species linked to severe childhood asthma. *Proc Natl Acad Sci U S A* **113**, 8997-9002 (2016).

7. Wright, M.H., Heal, W.P., Mann, D.J. & Tate, E.W. Protein myristoylation in health and disease. *J Chem Biol* **3**, 19-35 (2010).
8. Marc, D., Masson, G., Girard, M. & van der Werf, S. Lack of myristoylation of poliovirus capsid polypeptide VP0 prevents the formation of virions or results in the assembly of noninfectious virus particles. *J Virol* **64**, 4099-4107 (1990).
9. Marc, D., Drugeon, G., Haenni, A.L., Girard, M. & van der Werf, S. Role of myristoylation of poliovirus capsid protein VP4 as determined by site-directed mutagenesis of its N-terminal sequence. *EMBO J* **8**, 2661-2668 (1989).
10. Marc, D., Girard, M. & van der Werf, S. A Gly1 to Ala substitution in poliovirus capsid protein VP0 blocks its myristoylation and prevents viral assembly. *J Gen Virol* **72 (Pt 5)**, 1151-1157 (1991).
11. Moscufo, N., Simons, J. & Chow, M. Myristoylation is important at multiple stages in poliovirus assembly. *J Virol* **65**, 2372-2380 (1991).
12. Ritzefeld, M., Wright, M.H. & Tate, E.W. New developments in probing and targeting protein acylation in malaria, leishmaniasis and African sleeping sickness. *Parasitology*, 1-18 (2017).
13. Thinon, E. *et al.* Global profiling of co- and post-translationally N-myristoylated proteomes in human cells. *Nat Commun* **5**, 4919 (2014).
14. Bell, A.S. *et al.* Selective inhibitors of protozoan protein N-myristoyltransferases as starting points for tropical disease medicinal chemistry programs. *PLoS Negl Trop Dis* **6**, e1625 (2012).
15. Brannigan, J.A. *et al.* N-myristoyltransferase from Leishmania donovani: structural and functional characterisation of a potential drug target for visceral leishmaniasis. *J Mol Biol* **396**, 985-999 (2010).
16. Goncalves, V. *et al.* Discovery of Plasmodium vivax N-myristoyltransferase inhibitors: screening, synthesis, and structural characterization of their binding mode. *J Med Chem* **55**, 3578-3582 (2012).
17. Scharfer, C. *et al.* Torsion angle preferences in druglike chemical space: a comprehensive guide. *J Med Chem* **56**, 2016-2028 (2013).
18. Goncalves, V. *et al.* A fluorescence-based assay for N-myristoyltransferase activity. *Anal Biochem* **421**, 342-344 (2012).
19. Wright, M.H. *et al.* Validation of N-myristoyltransferase as an antimalarial drug target using an integrated chemical biology approach. *Nat Chem* **6**, 112-121 (2014).

20. Thinon, E., Morales-Sanfrutos, J., Mann, D.J. & Tate, E.W. N-Myristoyltransferase Inhibition Induces ER-Stress, Cell Cycle Arrest, and Apoptosis in Cancer Cells. *ACS Chem Biol* **11**, 2165-2176 (2016).
21. Broncel, M. *et al.* Multifunctional reagents for quantitative proteome-wide analysis of protein modification in human cells and dynamic profiling of protein lipidation during vertebrate development. *Angew Chem Int Ed Engl* **54**, 5948-5951 (2015).
22. Broncel, M. *et al.* Myristoylation profiling in human cells and zebrafish. *Data Brief* **4**, 379-383 (2015).
23. Tyanova, S., Temu, T. & Cox, J. The MaxQuant computational platform for mass spectrometry-based shotgun proteomics. *Nat Protoc* **11**, 2301-2319 (2016).
24. Reddel, H.K. *et al.* A summary of the new GINA strategy: a roadmap to asthma control. *Eur Respir J* **46**, 622-639 (2015).
25. Lee, W.M., Monroe, S.S. & Rueckert, R.R. Role of maturation cleavage in infectivity of picornaviruses: activation of an infectosome. *J Virol* **67**, 2110-2122 (1993).
26. Koh, C. *et al.* Oral prenylation inhibition with lonafarnib in chronic hepatitis D infection: a proof-of-concept randomised, double-blind, placebo-controlled phase 2A trial. *Lancet Infect Dis* **15**, 1167-1174 (2015).
27. Vizcaino, J.A. *et al.* ProteomeXchange provides globally coordinated proteomics data submission and dissemination. *Nat Biotechnol* **32**, 223-226 (2014).

Acknowledgments

The authors gratefully acknowledge financial support from the Medical Research Council (MRC) of the United Kingdom (grants G0900278 and a confidence in concept award to Imperial College, MC-PC-14100), the EPSRC (grant EP/F500416/1), Cancer Research UK (grant C29637/A20183), MRC-Asthma UK Centre in Allergic Mechanisms of Asthma (grant G1000758), and Imperial Innovations. AM is supported by an MRF/Asthma UK Research Grant (MRFAUK-

2015-311). SLJ is supported by a Chair from Asthma UK (CH11SJ) and is a National Institute of Health Research (NIHR) Senior Investigator. The Pirbright Institute receives strategic funding from the Biotechnology and Biological Research Council (BBSRC) of the United Kingdom. We thank Diamond Light Source for access to beamlines I04 and I04-1 (proposal numbers mx12579, mx7864 and mx9948). We thank Ernesto Cota (Imperial College London) for providing advice on structure determination, and Shirley Roberts for expert crystal handling. The authors thank Karl-Klaus Conzelmann (Max von Pettenkofer-Institut) for permission to use the BSR-T7/5 cell line.

Correspondence and requests for materials may be addressed to E.W.T. (e.tate@imperial.ac.uk) or R.S. (r.solari@imperial.ac.uk).

Author Contributions

A.M. and D.P.S. designed and executed rhinovirus infection experiments, with assistance from A.G. and R.S.; A.B. designed and synthesized NMT inhibitors, with E.W.T., J.A.H. and R.J.L.; J.N., A.A. and T.T. undertook poliovirus and foot-and-mouth disease virus infections, and sucrose gradient fractionation. J.M.S. undertook chemical proteomics experiments and data analysis, with E.W.T.; I.P.D, J.A.B. and A.J.W. undertook protein purification, X-ray crystallography and structure refinement. M.R. undertook cell viability and tagging experiments. S.W.R. and I.H.N. undertook SPR experiments and data analysis. S.L.J. provided advice on virus experiments, and access to essential facilities. E.W.T. and R.S. conceived the project and, with A.M. and A.B., directed the project. All authors contributed to writing of the manuscript.

Competing Financial Interests Statement

A.B., E.W.T., R.J.L., J.A.H. and J.A.B. are inventors on a patent application describing NMT inhibitors including IMP-1031 and IMP-1088 (Bell, A.S.; Tate, E.W.; Leatherbarrow, R.J.; Hutton, J.A.; Brannigan, J.A., “Compounds and their use as inhibitors of *N*-myristoyl transferase”, PCT In Appl (2017) WO 2017001812).

Figure 1: Proposed pathway for generation of infectious rhinovirus particles in an infected host cell. (**a**) Rhinovirus polyprotein is synthesized in the host, where it undergoes co-translational N-terminal methionine excision by host methionine aminopeptidase (MetAP) to reveal an N-terminal glycine, followed by N-terminal *N*-myristoylation by host NMT. (**b**) Capsid assembly starts with cleavage into VP0, VP3 and VP1 by RV protease, and assembly into protomers; protomers then assemble into pentamers, and then into an icosahedral capsid enclosing the RV RNA genome; finally, VP0 is processed into VP4 and VP2, and mature infectious virions are released.

Figure 2: Structure-guided discovery of potent human *N*-myristoyltransferase inhibitors. (**a**) Structures of hit compound IMP-72 and methylated analogue IMP-994, reconstructed fragment IMP-358 and fragment-linked compound IMP-917, and associated inhibitory activity (IC_{50}) on human NMT1 (HsNMT1). (**b**) Binding mode of IMP-72 in *Plasmodium vivax* NMT (PvNMT) determined to 1.69 Å resolution, in the presence of NHM (PDB: 5O48). Atoms colored by element: oxygen, red; nitrogen, blue; carbon, ice blue (inhibitor) and grey (protein); fluorine, purple. NHM, protein main chain and solvent molecules have been omitted for clarity, and polar protein-inhibitor interactions are shown by dashed lines. (**c**) Quaternary complex of PvNMT, NHM, IMP-72 and IMP-358 (PDB: 5O4V) determined to 1.7 Å resolution, with IMP-358 colored in lemon. (**d**) Binding sites for NHM, IMP-72 and IMP-358, in the context of the overall structure of PvNMT. The protein is a ribbon color-ramped from the N-terminus (blue) to the C-terminus (red). NHM, IMP-72 and IMP-358 are shown in space-filling representation colored by atom type (phosphorus, magenta) and distinguished by carbon atoms shown in grey, ice-blue and lemon, respectively.

(**e**) Binding mode of IMP-917 in human NMT1 (HsNMT1) with Myr-CoA (PDB 5O6H) determined to 1.29 Å resolution. Carbon atoms of the IMP-917 indazole core are colored ice blue, while those of the pendant trimethylpyrazole-containing species are lemon. See Supplementary Fig. 1 for ligand electron density maps.

Figure 3: Potent inhibitors of human *N*-myristoyltransferases inhibit rhinovirus myristoylation in infected cells. (**a**) Structures of IMP-1088 and IMP-1031, and *in vitro* inhibitory activity (IC_{50}) on human NMT1 (HsNMT1) and NMT2 (HsNMT2). (**b**) Binding mode of IMP-1088 in the ternary complex with human NMT1 and Myr-CoA (PDB: 5MU6), determined to 1.88 Å resolution, colored as in Fig. 2e. (**c**) Analysis of protein myristoylation in HeLa cells infected with rhinovirus RV-A16 (MOI 20) in presence of YnMyr, following ligation to TAMRA/Biotin azido capture reagent AzTB; red arrow: band of increased fluorescence intensity upon infection, corresponding to VP0. (**d**) Quantitative proteomic analysis of inhibition of protein myristoylation in RV-A16-infected HeLa cells (6 hours) by IMP-1088, following ligation to AzRB and enrichment on NeutrAvidin-agarose beads. Two-sample *t*-test (permutation-based false discovery rate (FDR), 250 permutations, FDR 0.01, S0=0.5) revealed significant changes in label-free quantification (LFQ) between 50 nM IMP-1088 and control (DMSO) for myristoylated proteins. Dashed lines: *t*-test significance cut off; red: RV-A16 proteins; blue: known co-translationally myristoylated host proteins[13]; white: other host proteins. Similar analyses were performed for the whole proteome (see Supplementary Fig. 3). (**e**) Western blot and in-gel fluorescence analysis of inhibition of VP0 myristoylation in HeLa cells infected with rhinovirus RV-A16 (MOI 20, 6 h) following recovery ligation to AzTB. Comparison of input protein, supernatant following pull-down on Streptavidin magnetic beads (Supnt) and eluted

proteins (Pull-down) demonstrates enrichment of YnMyr-tagged VP0, and specific inhibition of myristoylation; HSP90: non-myristoylated loading control.

Figure 4: Novel human *N*-myristoyltransferase inhibitors potently and efficiently block rhinovirus replication without cytotoxicity. (**a**) Multicycle rhinovirus replication assay. HeLa cells were infected with rhinovirus RV-A16 (MOI 0.5) for 2 days, and virus replication measured by the induced cytopathic effect (%CPE) for each inhibitor relative to vehicle (DMSO)-treated infected control, and uninfected controls. Error bars: SEM, n=3. (**b**) Cell viability in presence of NMT inhibitors for uninfected HeLa cells, as percentage of vehicle-treated control. Error bars: SEM, n=3. (**c**) and (**d**) Inhibition of single cycle replication in HeLa cells infected with rhinovirus RV-A16 (MOI 20) (**c**), or the indicated rhinovirus serotypes (**d**), for 6 h with indicated concentrations of IMP-1088; virus titers determined by endpoint dilution assay. $TCID_{50}$: 50% Tissue Culture Infective Dose, error bars: SEM, n=4 for (**c**) and n=3 for (**d**), ****: $p<0.0001$ (two-way ANOVA with Sidak's multiple comparisons test on $\log_{10}(TCID_{50}/ml)$). (**e**) Inhibition of single cycle replication in primary human bronchial epithelial cells (hBECs) infected with rhinovirus RV-A1 (MOI 5) for 7 h by IMP-1088; virus titers determined as in (**c**)/(**d**). Error bars: SEM, n=4. (**f**) Inhibitory effect of IMP-1088 added at different times post-infection, in a single cycle replication assay. HeLa cells were infected with rhinovirus RV-A16 (MOI 20) for 6 h and IMP-1088 (500 nM) added at the indicated times (+/- hours) relative to the time point of virus adsorption. Error bars: SEM, n=3, **: $p=0.0013$, ****: $p<0.0001$ (one-way ANOVA with Dunnett's multiple comparisons test on $\log_{10}(TCID_{50}/ml)$ against the DMSO control).

Figure 5: IMP-1088 inhibits production of infectious rhinovirus particles by blocking virus assembly. (**a**-**d**) Effect of IMP-1088 on rhinovirus replication kinetics in HeLa cells infected with rhinovirus RV-A16 (MOI 20) for 6 h in presence of IMP-1088 (500 nM) or DMSO (vehicle). At the indicated time points cell, lysates were analyzed for virus titer by endpoint titration (**a**), viral RNA by quantitative PCR (**b**) or viral protein levels by Western blot with an antibody directed against rhinovirus non-structural protein 2C ((**c**) and (**d**)). (**c**) Representative images of one of three independent repeats. (**d**) Quantification of signal corresponding to 2C protein, relative to Lamin B1 loading control, expressed as a percentage of 6 h DMSO control. Error bars: SEM, n=3. (**e**) Effect of IMP-1088 on rhinovirus capsid assembly. HeLa cells were infected with rhinovirus RV-A16 for 6 h in presence of IMP-1088 (500 nM) or DMSO (vehicle). Cell lysates were sedimented on sucrose density gradients and the fractions analyzed by Western blot with antibodies raised against whole rhinovirus RV-A16 capsids. (**f**) Densitometric analysis of (**e**), with indication of fractions in which controls sedimented (intact virion, empty capsid or monomer/pentamer).

a. Rhinovirus polyprotein synthesis and *N*-myristoylation by host biosynthetic machinery

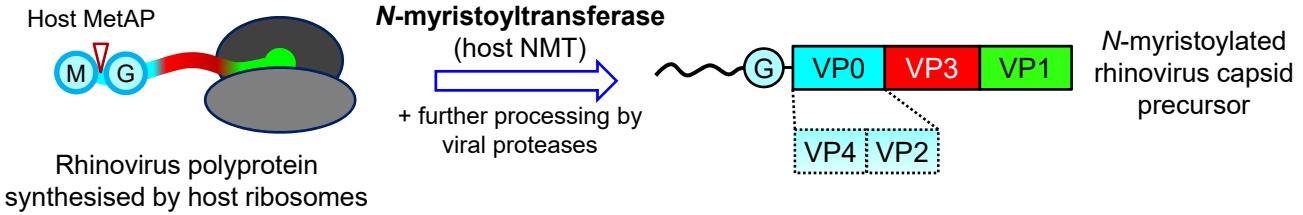

b. Rhinovirus capsid assembly and maturation

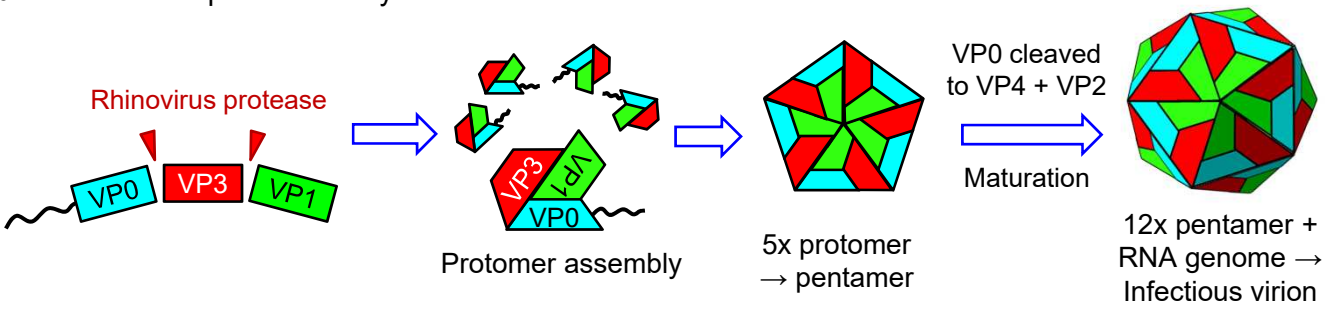

a

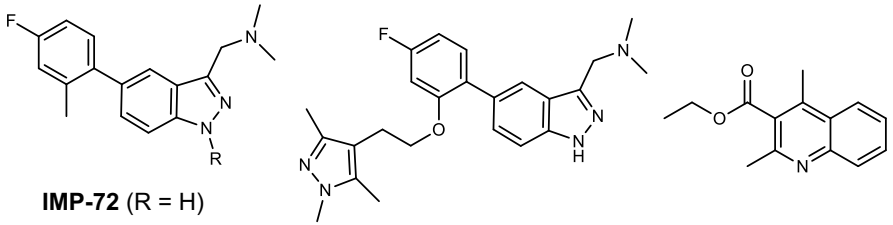

IMP-72 (R = H)
IMP-994 (R = Me)

IMP-917

IMP-358

Compound	HsNMT1 IC_{50}/μM
IMP-72	20
IMP-994	9
IMP-917	0.013
IMP-358	17% inhibition at 100 μM

b

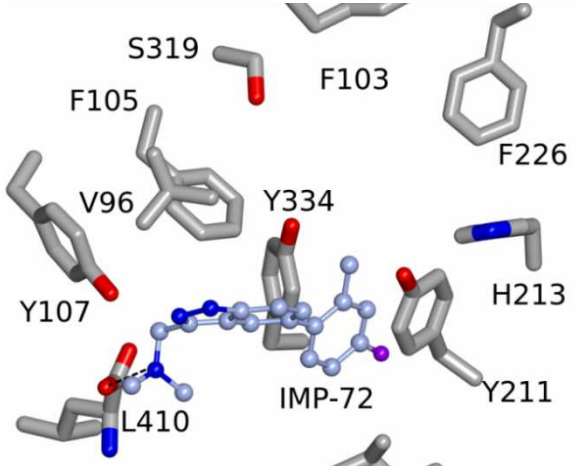

c

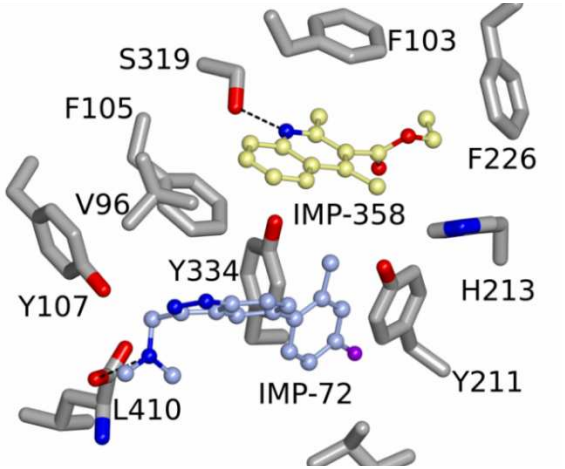

d

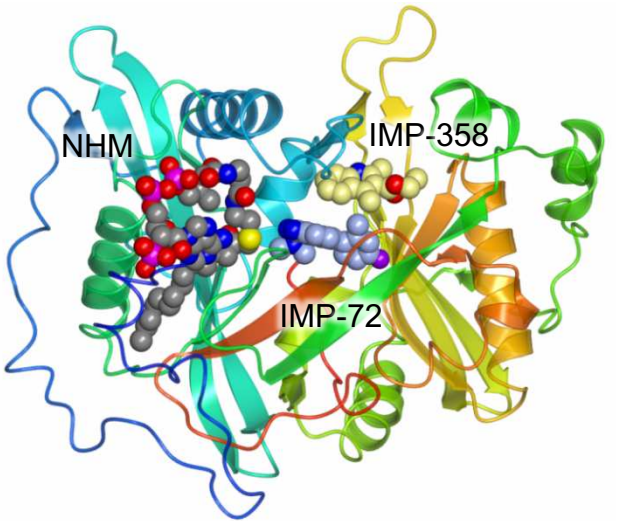

e

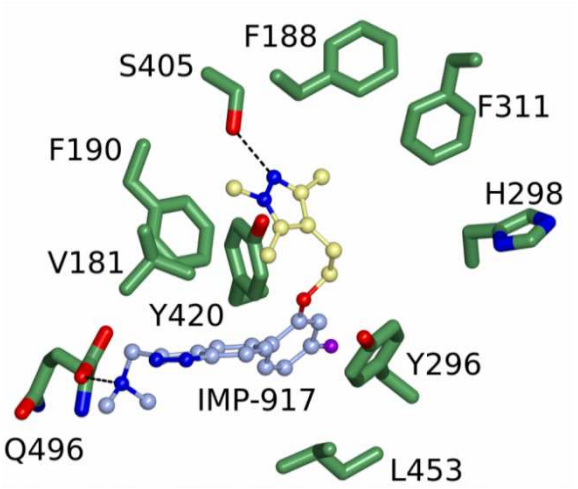

Figure 3

a

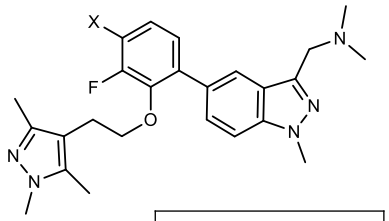

Compound	X	IC_{50}/nM HsNMT1	IC_{50}/nM HsNMT2
IMP-1031	H	4.6	2.8
IMP-1088	F	<1	<1

IMP-1088 K_d (HsNMT1) ≤ 210 pM

b

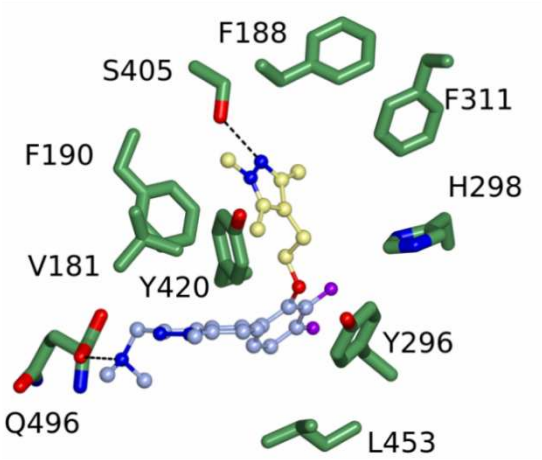

c

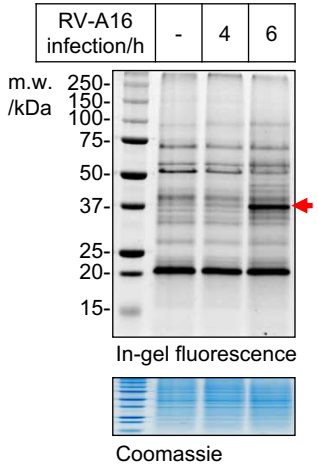

d

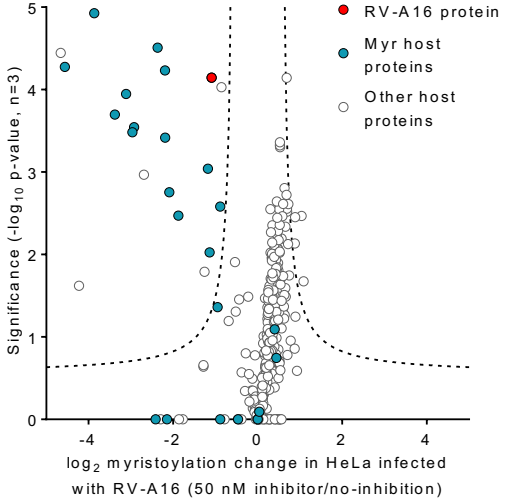

e

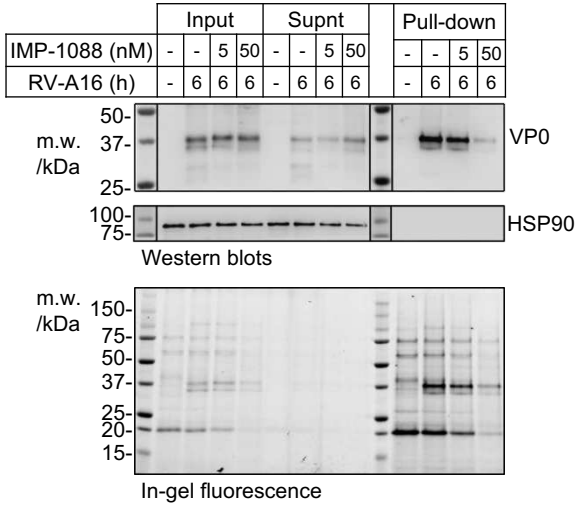

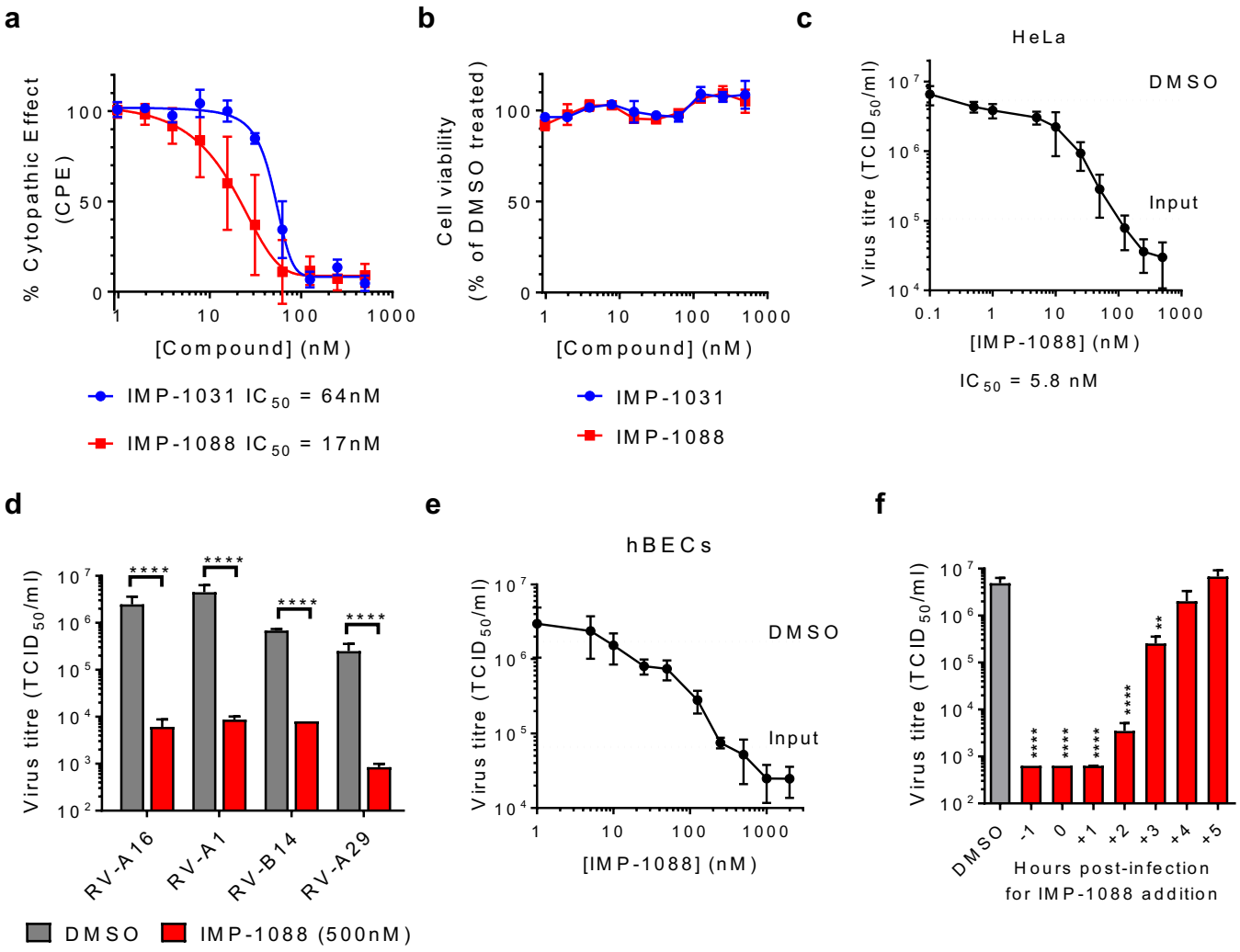
a
% Cytopathic Effect (CPE)
100
50
0
1
10
100
1000
[Compound] (nM)
IMP-1031 IC50 = 64nM
IMP-1088 IC50 = 17nM
b
Cell viability (% of DMSO treated)
100
50
0
1
10
100
1000
[Compound] (nM)
IMP-1031
IMP-1088
c
HeLa
DMSO
Input
Virus titre (TCID50/ml)
10 7
10 6
10 5
10 4
0.1
1
10
100
1000
[IMP-1088] (nM)
IC50 = 5.8 nM
d
Virus titre (TCID50/ml)
10 7
10 6
10 5
10 4
10 3
10 2
****
****
****
****
RV-A16
RV-A1
RV-B14
RV-A29
DMSO
IMP-1088 (500nM)
e
hBECs
DMSO
Input
Virus titre (TCID50/ml)
10 7
10 6
10 5
10 4
1
10
100
1000
[IMP-1088] (nM)
f
Virus titre (TCID50/ml)
10 7
10 6
10 5
10 4
10 3
10 2
****
****
****
****
**
DMSO
-1
0
+1
+2
+3
+4
+5
Hours post-infection
for IMP-1088 addition

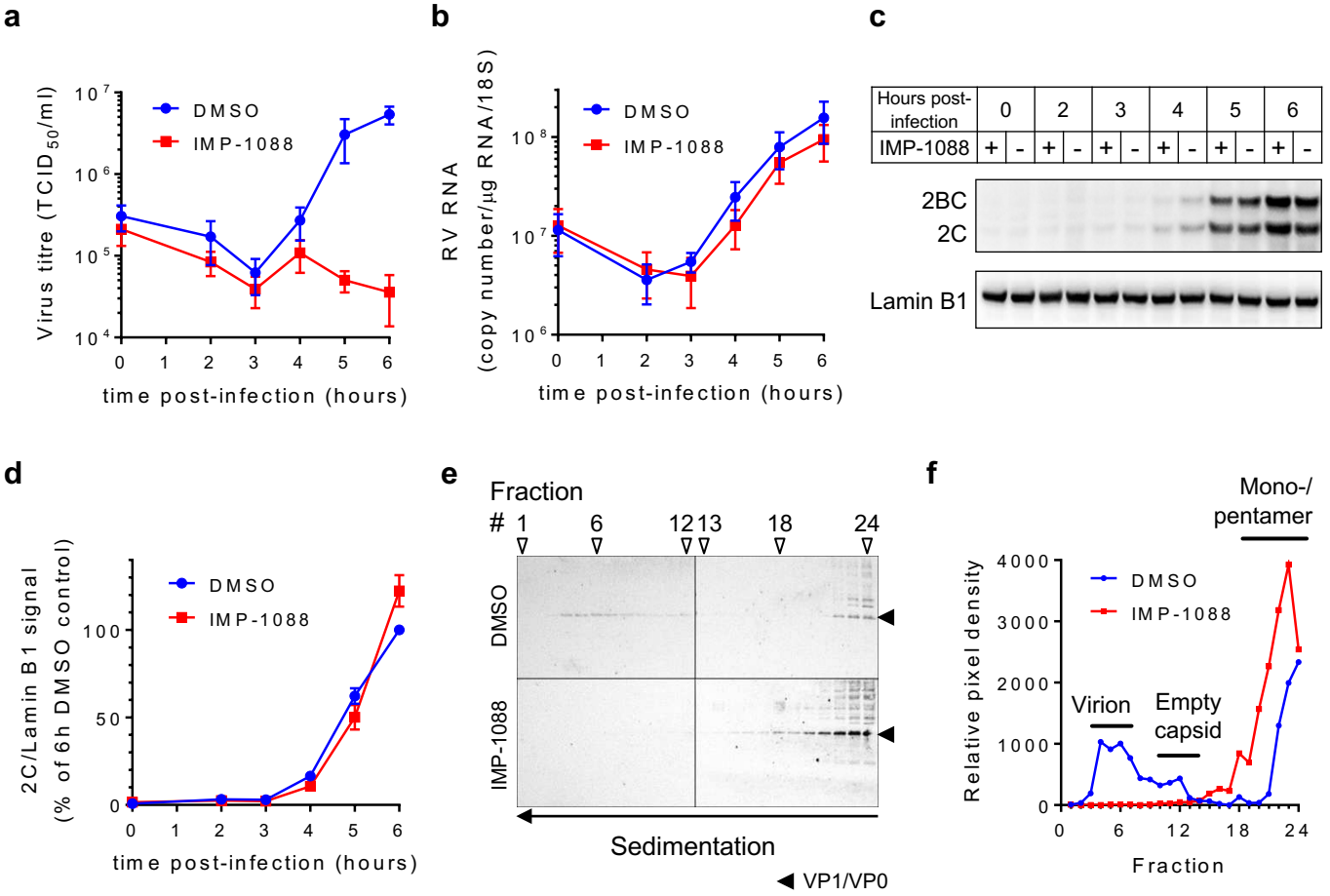
a
Virus titre (TCID50/ml)
DMSO
IMP-1088
time post-infection (hours)
b
RV RNA (copy number/µg RNA/18S)
DMSO
IMP-1088
time post-infection (hours)
c
Hours post-infection
0 2 3 4 5 6
IMP-1088
+ - + - + - + - + - + -
2BC
2C
Lamin B1
d
2C/Lamin B1 signal (% of 6h DMSO control)
DMSO
IMP-1088
time post-infection (hours)
e
Fraction
1 6 12 13 18 24
DMSO
IMP-1088
Sedimentation
VP1/VP0
f
Mono-/ pentamer
Relative pixel density
DMSO
IMP-1088
Virion
Empty capsid
Fraction

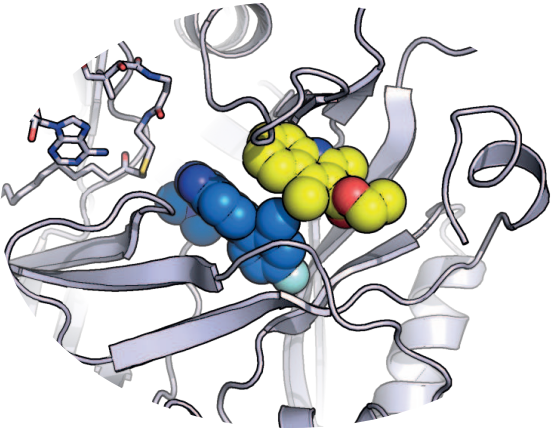

Fragment
reconstruction

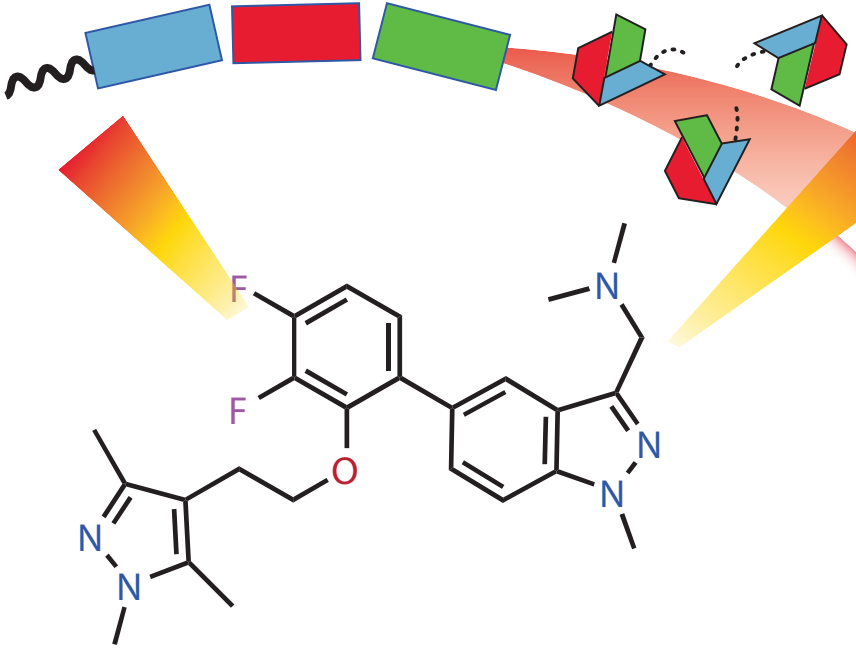

IMP-1088
Picomolar human NMT inhibitor

Potent
antiviral